

MIT Open Access Articles

Fundamental time scales of bubble fragmentation in homogeneous isotropic turbulence

The MIT Faculty has made this article openly available. **Please share** how this access benefits you. Your story matters.

Citation: Gaylo DB, Hendrickson K, Yue DKP. Fundamental time scales of bubble fragmentation in homogeneous isotropic turbulence. *Journal of Fluid Mechanics*. 2023;962:A25.

As Published: 10.1017/jfm.2023.281

Publisher: Cambridge University Press

Persistent URL: <https://hdl.handle.net/1721.1/155739>

Version: Author's final manuscript: final author's manuscript post peer review, without publisher's formatting or copy editing

Terms of use: Creative Commons Attribution-Noncommercial-ShareAlike



Banner appropriate to article type will appear here in typeset article

1 **Fundamental timescales of bubble fragmentation in** 2 **homogeneous isotropic turbulence**

3 **Declan B. Gaylo¹, Kelli Hendrickson¹ and Dick K. P. Yue¹†**

4 ¹Department of Mechanical Engineering, Massachusetts Institute of Technology, Cambridge, MA 02139,
5 USA

6 (Received xx; revised xx; accepted xx)

7 We investigate the fundamental timescales that characterise the statistics of fragmentation
8 under homogeneous isotropic turbulence (HIT) for air-water bubbly flows at moderate to
9 large bubble Weber numbers, We . We elucidate three timescales: τ_r , the characteristic age
10 of bubbles when their subsequent statistics become stationary; τ_ℓ , the expected lifetime of
11 a bubble before further fragmentation; and τ_c , the expected time for the air within a bubble
12 to reach the Hinze scale, radius a_H , through the fragmentation cascade. The timescale
13 τ_ℓ is important to the population balance equation (PBE), τ_r is critical to evaluating the
14 applicability of the PBE no-hysteresis assumption, and τ_c provides the characteristic time for
15 fragmentation cascades to equilibrate. By identifying a non-dimensionalized average speed
16 \bar{s} at which air moves through the cascade, we derive $\tau_c = C_\tau \varepsilon^{-1/3} a^{2/3} (1 - (a_{max}/a_H)^{-2/3})$,
17 where $C_\tau = 1/\bar{s}$ and a_{max} is the largest bubble radius in the cascade. While \bar{s} is a function
18 of PBE fragmentation statistics, which depend on the measurement interval T , \bar{s} itself is
19 independent of T for $\tau_r \ll T \ll \tau_c$. We verify the T -independence of \bar{s} and its direct
20 relationship to τ_c using Monte Carlo. We perform direct numerical simulations (DNS) at
21 moderate to large bubble Weber numbers, We , to measure fragmentation statistics over a
22 range of T . We establish that non-stationary effects decay exponentially with T , independent
23 of We , and provide $\tau_r = C_r \varepsilon^{-1/3} a^{2/3}$ with $C_r \approx 0.11$. This gives $\tau_r \ll \tau_\ell$, validating the
24 PBE no-hysteresis assumption. From DNS, we measure \bar{s} and find that for large Weber
25 numbers ($We > 30$), $C_\tau \approx 9$. In addition to providing τ_c , this obtains a new constraint on
26 fragmentation models for PBE.

27 **Key words:**

28 **1. Introduction**

29 Fragmentation of bubbles by turbulence resulting in transfer of volume from large to small
30 scales through a fragmentation cascade is relevant to a variety of natural and engineering
31 applications. We consider air-water turbulent bubbly flows where the density ratio between
32 that of the bubble (ρ_a) and the surrounding fluid (ρ_w) is $\rho_w/\rho_a \sim 1000$. While these
33 flows often exhibit multiple physical processes that affect the number of bubbles of a given

† Email address for correspondence: yue@mit.edu

size (e.g., entrainment, degassing, dissolution, coalescence), fragmentation is critical to understanding the size-distribution of bubbles. For typical bubbly flows with macroscopic timescales large compared to those of the underlying turbulence, the distribution of large bubbles often matches an equilibrium fragmentation cascade (Garrett *et al.* 2000; Deane & Stokes 2002; Deike 2022), suggesting that fragmentation dominates and rapidly reaches equilibrium. Applicable to flows with large Reynolds numbers where the length scale of the bubbles is much larger than the Kolmogorov scale but much smaller than the geometric length scales of the flow, fragmentation of bubbles within the Kolmogorov inertial sub-range of homogeneous isotropic turbulence (HIT) is often studied. Recent work has shown that HIT is observed at the bubble scale even in close proximity to a free surface (Yu *et al.* 2019).

In HIT, fragmentation is primarily governed by the disturbing effect of turbulent fluctuations and the restoring effect of surface tension. The ratio between the two is given by the bubble Weber number

$$We = \frac{2\varepsilon^{2/3}(2a)^{5/3}}{(\sigma/\rho_w)}, \quad (1.1)$$

where ε is the turbulent dissipation rate, a is the parent-bubble radius, and σ is the surface-tension coefficient. As bubbles are not generally spherical, radius, a , of a bubble here is defined in terms of the volume, v , of the bubble by $a = (3v/4\pi)^{1/3}$. The Hinze scale is defined as the Weber number We_H (and corresponding radius a_H) below which surface tension largely prevents fragmentation (Hinze 1955). Thus, our focus is moderate ($We \gtrsim We_H$) to large ($We \gg We_H$) Weber numbers where fragmentation is present.

For $We \sim \infty$, the daughter bubbles of a previous fragmentation will themselves fragment, leading to an *equilibrium* fragmentation cascade with bubble-size distribution $N(a) \propto a^{-10/3}$ (Garrett *et al.* 2000). Here, $N(a)\delta a$ is defined to be the number of bubbles of radius $a \leq a' < a + \delta a$. Using location as an analogy for bubble size, for finite We the flux of air due to fragmentation can be either local, corresponding to daughter bubbles of similar size as the parent bubble and likely to further fragment, or non-local, corresponding to daughters much smaller than the parent and likely smaller than a_H (Chan *et al.* 2021*b*). Chan *et al.* (2021*c*) measure bubbles $We \sim 20$ and demonstrate the locality of the majority of the flux, confirming the applicability of the fragmentation cascade and associated $-10/3$ power law for moderate and large We , where surface tension is present but does not prevent fragmentation. This $-10/3$ power law is observed in a variety of flows including emulsions (Skartlien *et al.* 2013), breaking waves (Deane & Stokes 2002), and turbulent free-surface entrainment (Yu *et al.* 2020). This prevalence illustrates that fragmentation cascades are ubiquitous to turbulent bubbly flows for $We > We_H$, and that, despite these flows being transient, an equilibrium fragmentation cascade is often obtained.

For $We > We_H$ where a cascade is formed, our interest here is the evolution of the bubble statistics, in particular the bubble-size distribution $N(a)$, due to fragmentation. In principle, this evolution can be derived from a (more) complete mechanistic description of fragmentation, which is a subject of active investigation (e.g., Liao & Lucas 2009; Qi *et al.* 2022; Rivière *et al.* 2021, 2022). In addition to the challenge of disparate mechanistic descriptions, another challenge is that these often describe the behaviour of a bubble as dependent on its history (for example, the two-step process presented by Rivière *et al.* (2022)). Contrarily, statistical modelling of bubble-size distributions, particularly through population balance equations (PBE) often used to model large-scale bubbly flows (e.g., Castro & Carrica 2013), assumes that the statistical behaviour of a bubble is independent of its history, i.e., no hysteresis. The present work complements mechanistic studies by focusing on the fundamental statistics of turbulent fragmentation, quantified through their characteristic timescales. While individual physical mechanisms can also be characterised by

82 timescales, such as the timescale for a sufficiently strong eddy to fragment a bubble (Qi *et al.*
 83 2022) or the timescale for capillary-driven production of sub-Hinze bubbles (Rivière *et al.*
 84 2021, 2022), our focus is on the timescales that characterise the fundamental statistics of
 85 fragmentation. Understanding these timescales will directly support the statistical modelling
 86 of bubble-size distributions through PBE. Additionally, the understanding provided by these
 87 statistical timescales will provide robust ways to compare disparate mechanistic models of
 88 fragmentation.

89 In this work, we elucidate and quantify three fundamental timescales of fragmentation for
 90 moderate to large- We HIT. In order of magnitude from small to large, these are: the bubble
 91 relaxation time τ_r which characterises the time from when a bubble is formed to when its
 92 subsequent dynamics (e.g., the rate of fragmentation) become statistically stationary, the
 93 (well-established) bubble lifetime τ_ℓ which characterises the time from when a bubble is
 94 formed to when it undergoes fragmentation (Martínez-Bazán *et al.* 1999a; Garrett *et al.*
 95 2000), and the convergence time τ_c which characterises the time needed for the air to go
 96 from the scale of the largest bubble, radius a_{max} , to the Hinze scale, a_H . In §2 we examine
 97 how these timescales relate to statistical modelling of bubble-size distributions through PBE.
 98 In previous work, τ_c could not be described for realistic fragmentation statistics (Deike
 99 *et al.* 2016; Qi *et al.* 2020). In §3 we develop a Lagrangian mathematical description which
 100 provides the speed at which volume moves through the fragmentation cascade. This volume-
 101 propagation speed allows us to derive τ_c for realistic fragmentation statistics at large We .
 102 We prove that, unlike typical fragmentation statistics, the volume-propagation speed can
 103 be obtained independent of the time interval used for measurement. In §4 we perform
 104 direct numerical simulations (DNS) of moderate- to large- We bubble fragmentation in HIT
 105 to quantify the three fundamental timescales we address. In §5 we discuss new insights
 106 provided by the quantification of these timescales: τ_r shows hysteresis can be neglected in
 107 PBE, and τ_c provides a new constraint on large- We fragmentation models.

108 2. Three fundamental timescales of fragmentation

109 To define characteristic timescales of fragmentation, we start by examining the statistics
 110 typically used to describe fragmentation. To model the population of bubbles within a flow,
 111 the evolution $(\partial N/\partial t)(a, t)$ is often expressed as a Boltzmann-style population balance
 112 equation (PBE) with source terms \mathcal{S} describing the effect of each evolution mechanism:
 113 fragmentation, coalescence, entrainment, etc. (Sporleder *et al.* 2012). For fragmentation, this
 114 source term is

$$115 \quad \mathcal{S}_f(a, t) = -\Omega(a)N(a, t) + \int_a^\infty \bar{m}(a')\beta(a; a')\Omega(a')N(a', t) da', \quad (2.1)$$

116 which includes three fragmentation statistics: $\Omega(a)$ is the fragmentation rate (units time^{-1}),
 117 $\bar{m}(a')$ is the average number of daughter bubbles created by fragmentation of a parent of
 118 radius a' , and $\beta(a; a')$ is the daughter-size distribution, expressed as a probability distribution
 119 function of daughter radius a for a given parent radius a' . As volume is conserved in an
 120 incompressible flow, it is useful to represent the daughter-size distribution in terms of a
 121 volume ratio $v^* = (a/a')^3$, giving a daughter-size distribution f_V^* related to β by

$$122 \quad a'\beta(a; a') = 3(v^*)^{2/3}f_V^*(v^*; a'). \quad (2.2)$$

123 Applying volume conservation, the distribution must satisfy (Martínez-Bazán *et al.* 2010)

$$124 \quad \bar{m}(a') \int_0^1 v^* f_V^*(v^*; a') dv^* = 1. \quad (2.3)$$

125 While there is great variety in models for $\bar{m}(a')$ and $\beta(a, a')$ (Liao & Lucas 2009), models
126 for $\Omega(a)$ generally follow

$$127 \quad \Omega(a) = C_{\Omega}(We)\varepsilon^{1/3}a^{-2/3}, \quad (2.4)$$

128 where $C_{\Omega}(We)$ approaches a constant value $C_{\Omega,\infty}$ as $We \rightarrow \infty$. Dimensional analysis
129 shows C_{Ω} may also depend on Reynolds number and an additional parameter, such as
130 the ratio between parent-bubble radius and the Kolmogorov scale, a/η , implied by Qi *et al.*
131 (2022); however, the power-law scaling in (2.4) is robust at large We (Martínez-Bazán
132 *et al.* 2010). Assuming $We \sim \infty$ to neglect surface tension, this scaling can be arrived at
133 mechanistically by dividing the characteristic velocity of the turbulent fluctuations on the
134 scale of a bubble ($\varepsilon^{1/3}a^{1/3}$) by the characteristic length a bubble must deform to fragment
135 (a) (Garrett *et al.* 2000). A model for moderate to large We based on the assumption that
136 the rate of fragmentation is proportional to the difference between the deforming force of
137 turbulent fluctuations and the restoring force of surface tension is

$$138 \quad C_{\Omega}(We) = C_{\Omega,\infty}\sqrt{1 - We_H/We}, \quad (2.5)$$

139 with $C_{\Omega,\infty} \approx 0.42$ (Martínez-Bazán *et al.* 1999a; Martínez-Bazán *et al.* 2010). To relate
140 $\Omega(a)$ to measured quantities, let $p_{\text{frag}}(a; T)$ be the probability of fragmentation over some
141 measurement interval T , i.e., the probability a bubble of radius a present at time t will
142 fragment before the next measurement at time $t + T$. If we assume, as is done in PBE, that
143 the fragmentation rate of a bubble is independent of the time since its formation, then

$$144 \quad p_{\text{frag}}(a; T) = 1 - \exp[-T\Omega(a)], \quad (2.6)$$

145 and the expected lifetime $\tau_{\ell} = 1/\Omega(a)$.

146 Returning to (2.1), we examine this assumption that the statistics describing fragmentation
147 are independent of bubble age, which we will refer to as the no-hysteresis assumption. This
148 no-hysteresis assumption means that the (statistical) behaviour of a bubble after it is created
149 by fragmentation should be indistinguishable from a bubble that has existed for a much
150 longer time. Physically, this seems unlikely over short timescales, as the young bubble must
151 be significantly deformed from equilibrium. Regardless of the mechanistic explanation for
152 fragmentation (either the result of accumulation of surface oscillations (Risso & Fabre 1998)
153 or a single-sufficiently strong eddy (Martínez-Bazán *et al.* 1999a)), we expect a young bubble
154 to be more likely to fragment, violating no-hysteresis.

155 For PBE modelling, it is desirable to assume the effect of hysteresis is negligible, as
156 this allows fragmentation to be treated as statistically independent events; however, as
157 expected, the validity of this no-hysteresis assumption depends on the timescale one uses to
158 define fragmentation events (Solsvik *et al.* 2016). As infinitely small temporal resolution is
159 unobtainable, a finite measurement interval T is inherent in the measurement of fragmentation
160 events from both experiments and simulations (Vejražka *et al.* 2018; Chan *et al.* 2021a).
161 To avoid making the no-hysteresis assumption, we will allow for measured fragmentation
162 statistics to depend on T . We rearrange (2.6) to define the T -dependent fragmentation rate

$$163 \quad \Omega(a; T) \equiv -\ln[1 - p_{\text{frag}}(a; T)]/T. \quad (2.7)$$

164 For large We where daughter bubbles will eventually fragment, it is clear that \bar{m} must also
165 depend on T , and therefore, by (2.3), so must f_V^* . Thus, let $\bar{m}(a'; T)$ be the expected number
166 of daughters present at $t + T$ if the bubble fragments and $f_V^*(v^*; a', T)$ be the size distribution
167 of these daughters. The dependence of these statistics on T makes them difficult to relate to
168 the statistics in (2.1) (Solsvik *et al.* 2016). Although the physical mechanism for the decay
169 of hysteresis is unclear, we posit that there exists a timescale τ_r characterising how long the

170 decay takes, such that $\Omega(a; T \gg \tau_r) = \Omega(a)$ is independent of T . It follows that $\tau_\ell \gg \tau_r$ is
 171 required for the no-hysteresis assumption to be valid in PBE.

172 When modelling the bubble-size distribution, the equilibrium solution ($\partial N / \partial t = 0$) may
 173 be available, such as for PBE with only a fragmentation source term (Garrett *et al.* 2000) or
 174 fragmentation with power-law entrainment, where the size distribution of the bubbles injected
 175 by entrainment follows a power law (Gaylo *et al.* 2021). The time, τ_c , it takes to reach these
 176 equilibrium solutions is of interest: if τ_c is much less than the timescale over which the flow
 177 is transient, we expect an equilibrium fragmentation cascade (generally $N(a) \propto a^{-10/3}$) to
 178 be obtained. Gaylo *et al.* (2021) provide an expression for τ_c which allows for arbitrary f_V^*
 179 and \bar{m} , but its derivation is specific to power-law entrainment. For general fragmentation
 180 cascades, τ_c is characterised by the time it takes for the volume of the largest bubble to
 181 reach the Hinze scale (Deike *et al.* 2016; Qi *et al.* 2020). This characterisation is useful
 182 because it allows τ_c to be measured independent of the evolution of $N(a)$. Additionally,
 183 being directly related to fragmentation, it could provide a constraint on the fragmentation
 184 statistics in PBE (Qi *et al.* 2020). However, current derivations of τ_c from fragmentation
 185 statistics assume that bubbles break into identically-sized daughters, ignoring the effect of
 186 f_V^* . Although Monte Carlo simulation can be used to determine what τ_c is predicted by given
 187 fragmentation statistics (Qi *et al.* 2020), the lack of a general analytic expression relating τ_c
 188 to realistic fragmentation statistics precludes the reverse – it is unclear how a given value of
 189 τ_c constrains fragmentation statistics.

190 3. Describing τ_c using a Lagrangian description of fragmentation cascades

191 In this section, we derive a general analytic expression that relates τ_c to realistic fragmentation
 192 statistics. Previous derivations of τ_c assume identical fragmentation and that the life of a
 193 bubble is exactly (rather than on the average) equal to τ_ℓ so that the cascade can be treated
 194 as a series of discrete deterministic fragmentation events (Deike *et al.* 2016). While this
 195 approach provides the general physical scaling of τ_c , it is unable directly relate τ_c to realistic
 196 fragmentation statistics. In this section we use a Lagrangian air particle-based mathematical
 197 description of the speed at which volume moves through fragmentation cascades to derive
 198 τ_c . We note that this is a “speed” in the abstract sense as it measures how quickly air moves
 199 from large bubbles to small bubbles through the fragmentation cascade rather than through
 200 physical space. However, this description is useful as, through this speed, τ_c can be related to
 201 realistic fragmentation statistics and this speed is also directly accessible from volume-based
 202 bubble-tracking (Gaylo *et al.* 2022). Although T -independence is obvious when τ_c is obtained
 203 through the evolution of $N(a)$, it is less clear when τ_c is obtained through fragmentation
 204 statistics, which generally depend on T . We show that our approach allows fragmentation
 205 statistics-based measurement of τ_c independent of T .

206 Throughout this section, we consider large We ($We \gg We_H$) so that we can assume that
 207 fragmentation statistics are scale-invariant and simplify (2.5) to a Heaviside step function:

$$208 \quad C_\Omega(We) = C_{\Omega, \infty} \mathcal{H}(1 - We_H / We) . \quad (3.1)$$

209 In the following derivation, we also assume no-hysteresis, limiting applicability to timescales
 210 much larger than τ_r .

211 3.1. A Lagrangian-based mathematical description of fragmentation

212 Previous work on the movement of volume in fragmentation cascades applies Eulerian
 213 descriptions, focusing on volume flux. To find the equilibrium between entrainment and
 214 fragmentation, Gaylo *et al.* (2021) balance the flux of volume in and out of the set of
 215 bubbles of a given range of sizes. To evaluate locality, Chan *et al.* (2021b) study the flux

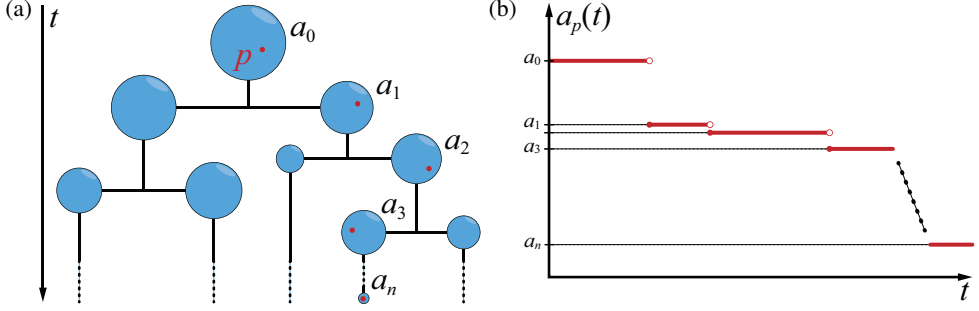


Figure 1: (a) Schematic of the Lagrangian description showing the path of a Lagrangian air particle p through a sequence of fragmentations from large to small radii, $a_0, a_1 \dots a_n$, of the bubble containing p ; and (b) the function $a_p(t)$ describing the evolution of this bubble radius. Describing the radius of the bubble containing p as a function of time allows a propagation speed of p through the cascade to be defined.

216 of volume from bubbles larger than a given size to those smaller. Eulerian descriptions are
 217 useful to model the volume flow in and out of specified bubble sizes, but to derive τ_c we
 218 need to understand how any specific air volume flows through the entire cascade. For this, a
 219 Lagrangian description is more direct.

220 Consider how a single Lagrangian particle of air p moves through a fragmentation cascade,
 221 illustrated in figure 1. Let $a_p(t)$ be the effective radius of the bubble that contains p at time
 222 t . Treating the interface between fluids as zero-thickness, one bubble breaks up into two
 223 instantaneously, thus $a_p(t)$ is a step function. From this $a_p(t)$, we have a simple expression
 224 for τ_c : Defining time for a particle such that $a_p(0) = a_{max}$, our interest is the expected time
 225 for p to reach the Hinze scale,

$$226 \quad \tau_c \equiv \mathbb{E} \{ \min \{ t : a_p(t) \leq a_H \} \} . \quad (3.2)$$

227 We now develop a relationship between this Lagrangian description and the previous
 228 fragmentation statistics. Incorporating the measurement interval T , we define the volume
 229 ratio between the bubble containing p at time t and the bubble containing p at time $t + T$:

$$230 \quad v_R(t; T) \equiv [a_p(t+T)/a_p(t)]^3 . \quad (3.3)$$

231 If the bubble containing p at time t does not fragment over the measurement interval T , then
 232 $v_R = 1$. If the bubble does fragment, then v_R depends on the size of the daughter bubble that
 233 p ends up in. Noting that the probability p ends up in a given daughter is equivalent to v^* , the
 234 ratio of the volume of the daughter to that of the parent, the probability distribution function
 235 for v_R given that fragmentation occurs, $f_{v_R | \text{frag}}$, is related to the previous fragmentation
 236 statistics through

$$237 \quad f_{v_R | \text{frag}}(v_R; t, T) = \bar{m}(a_p(t); T) v_R f_V^*(v_R; a_p(t), T) . \quad (3.4)$$

238 We assume these statistics are scale invariant and introduce the non-dimensional parameter
 239 $T^* = T \varepsilon^{1/3} a_p(t)^{-2/3}$. This gives

$$240 \quad f_{v_R | \text{frag}}(v_R; T^*) = \bar{m}(T^*) v_R f_V^*(v_R; T^*) , \quad (3.5)$$

241 and any moment n of the distribution is given by

$$242 \quad \mathbb{E} \{ [v_R(T^*)]^n \mid \text{frag} \} = \bar{m}(T^*) \int_0^1 v^{*n+1} f_V^*(v^*; T^*) dv^* . \quad (3.6)$$

3.2. Defining the volume-propagation speed in a fragmentation cascade

243

244 To obtain τ_c , we derive a metric that measures the speed at which Lagrangian air particles
 245 move through fragmentation cascades. To derive a speed, we must first define the “location”,
 246 $x(t)$, of a Lagrangian air particle p within the cascade. In this case location refers to some
 247 scalar bubble-size metric within the cascade rather than a physical spatial coordinate. We
 248 define $x(t)$ to describe the location of p within the fragmentation cascade such that the
 249 associated speed $s(t) \equiv \dot{x}(t)$ is constant for $a_p(t) > a_H$. A constant speed is necessary for
 250 many of the properties that will follow and, as a result of the scaling in (2.4), is achieved
 251 only by $x(t) \propto a_p(t)^{2/3}$. We choose

$$252 \quad x(t) \equiv -\varepsilon^{-1/3} a_p(t)^{2/3}, \quad (3.7)$$

253 which has dimensions of time, so that, in addition to being constant, the time-derivative of
 254 $x(t)$,

$$255 \quad s(t) = -\frac{2}{3} \varepsilon^{-1/3} a_p(t)^{-1/3} \frac{d}{dt} a_p(t), \quad (3.8)$$

256 is also positive and non-dimensional.

257 Because $a_p(t)$ is a step function, the derivative in (3.8) is ill-behaved. Thus, to evaluate
 258 $s(t)$ we consider its time-averaged value over a measurement interval T ,

$$259 \quad \langle s(t) \rangle_T \equiv \frac{1}{T} \int_t^{t+T} s(t') dt'. \quad (3.9)$$

260 This gives

$$261 \quad \langle s(t) \rangle_T = \frac{x(t+T) - x(t)}{T} = \frac{\varepsilon^{-1/3} a_p(t)^{2/3}}{T} \left(1 - [v_R(t; T)]^{2/9} \right), \quad (3.10)$$

262 where (3.3) defines the volume ratio $v_R(t; T)$. Furthermore, we perform an ensemble average
 263 to get $\mathbb{E} \{ \langle s(t) \rangle_T \}$, the expected time-averaged speed for an ensemble of (independent)
 264 Lagrangian air particles. Noting that $\langle s(t) \rangle_T = 0$ if no fragmentation occurs over the interval
 265 T ,

$$266 \quad \mathbb{E} \{ \langle s(t) \rangle_T \} = \frac{p_{\text{frag}}(a_p(t); T)}{\varepsilon^{1/3} a_p(t)^{-2/3} T} \left(1 - \mathbb{E} \{ [v_R(t; T)]^{2/9} \mid \text{frag} \} \right). \quad (3.11)$$

267 The no-hysteresis assumption, along with (2.4), gives

$$268 \quad \mathbb{E} \{ \langle s(t) \rangle_T \} = C_\Omega (We) \frac{1 - \exp[-\Omega(a_p(t)T)]}{\Omega(a_p(t)T)} \left(1 - \mathbb{E} \{ [v_R(t; T)]^{2/9} \mid \text{frag} \} \right). \quad (3.12)$$

269 Recalling that, by assumption, these statistics are scale invariant, we introduce T^* and apply
 270 (3.6) to obtain

$$271 \quad \mathbb{E} \{ \langle s(t) \rangle_{T^*} \} = C_{\Omega, \infty} \frac{1 - \exp[-C_{\Omega, \infty} T^*]}{C_{\Omega, \infty} T^*} \left[1 - \bar{m}(T^*) \int_0^1 v^{*11/9} f_V^*(v^*; T^*) dv^* \right]. \quad (3.13)$$

272 The limit $T^* \rightarrow 0$ gives the expected instantaneous speed,

$$273 \quad \bar{s} \equiv \lim_{T^* \rightarrow 0} \mathbb{E} \{ \langle s(t) \rangle_{T^*} \} = C_{\Omega, \infty} \left[1 - \bar{m} \int_0^1 v^{*11/9} f_V^*(v^*) dv^* \right], \quad (3.14)$$

274 where \bar{m} and $f_V^*(v^*)$ describe the fragmentation statistics for $T^* \rightarrow 0$ and are equivalent to
 275 those in (2.1).

276 Hereafter, we refer to \bar{s} as the volume-propagation speed of a fragmentation cascade.
 277 Although the size locations of individual Lagrangian air particles in the cascade follow step

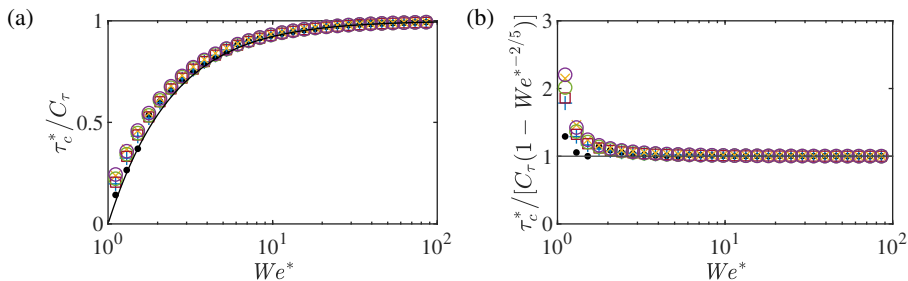


Figure 2: The effect of We^* on τ_c^* as modelled by (3.16) (—) compared to Monte Carlo simulations of daughter distributions, \bullet , A; $+$, B; \times , C; \square , D; \circ , E; \diamond , F (see table 1), where (3.1) is used to model the Hinze scale. The 95% C.I. on all τ_c^* is $< 1\%$.

278 functions, by commuting time averaging and ensemble averaging, we are able to obtain
 279 an average instantaneous speed for particles in the cascade. This speed \bar{s} can be related to
 280 fragmentation statistics measured over finite intervals T (3.13), or the instantaneous statistics
 281 used by PBE (3.14). The relationship between the two is explored in §3.4. In §3.3 we use \bar{s}
 282 to provide τ_c .

283 3.3. Describing convergence time, τ_c

284 As intended, our choice of the definition of location within the cascade, $x(t)$, makes \bar{s} constant
 285 for $a_p(t) > a_H$. This constant speed means that, despite $x(t)$ being a step function, after a
 286 sufficient number of steps, we can treat fragmentation as a continuous process and apply the
 287 approximation $x(t) \approx t\bar{s}$ with reasonable (statistical) accuracy. Thus, we can approximate τ_c
 288 as the distance in x between a_{max} and a_H divided by this speed,

$$289 \tau_c = \frac{(\varepsilon^{-1/3} a_{max}^{2/3}) - (\varepsilon^{-1/3} a_H^{2/3})}{\bar{s}}. \quad (3.15)$$

290 Non-dimensionalizing $\tau_c^* = \tau_c \varepsilon^{1/3} a_{max}^{-2/3}$ and defining We_{max} to be the We associated
 291 with a_{max} ,

$$292 \tau_c^* = C_\tau \left[1 - (We_{max}/We_H)^{-2/5} \right]; \quad C_\tau \equiv 1/\bar{s}. \quad (3.16a, b)$$

293 Despite the approximation used to derive (3.15) from \bar{s} in (3.14), (3.16) is expected
 294 to be valid for $We^* = We_{max}/We_H$ not small (where multiple fragmentation events are
 295 generally necessary to reach a_H). This is confirmed by Monte Carlo simulations of prescribed
 296 fragmentation statistics (figure 2).

297 For $We \sim \infty$ we recover the same $\tau_c \propto \varepsilon^{-1/3} a_{max}^{2/3}$ scaling as previous work which
 298 assumes identical fragmentation (Deike *et al.* 2016). This scaling of τ_c is like τ_ℓ , demon-
 299 strating that the fragmentation rate is a dominant factor in determining τ_c . Our propagation
 300 speed-based analysis provides the scaling constant C_τ which quantifies the contribution of
 301 fragmentation rate, as well as fragmentation statistics \bar{m} and $f_V^*(v^*)$. For large-but-finite We ,
 302 (3.16) captures the effect of the We -driven separation between a_{max} and a_H on the value
 303 of τ_c ; however, we note that the scaling of τ_c with We will be more complex for small We
 304 ($We \sim We_H$) as we have not incorporated the effect of finite- We on fragmentation rate, such
 305 as modelled by (2.5), into our propagation speed-based analysis. In §4.5, DNS shows for
 306 what sufficiently-large We this effect is negligible.

307 Although primarily driven by fragmentation rate, τ_c is also related to the fragmentation
 308 statistics \bar{m} and $f_V^*(v^*)$ (Qi *et al.* 2020), which is now quantified by the scaling constant C_τ .
 309 To describe these relationships, we follow Gaylo *et al.* (2021) and isolate the effect of f_V^*

Label	Daughter Distribution	m	$f_V^*(v^*)$	C_f	C_f^*
A	Valentas <i>et al.</i> (1966)	2	$\delta(v^* - 1/2)$	1	1
B	Martínez-Bazán <i>et al.</i> (1999b)	2	$(v^*)^{2/9} (1 - v^*)^{2/9}$	1.348	1.314
C	Tsouris & Tavlarides (1994)	2	$2^{1/3} - (v^*)^{2/3} - (1 - v^*)^{2/3}$	2.432	2.255
D	Martínez-Bazán <i>et al.</i> (2010)	2	$(v^*)^{-4/9} (1 - v^*)^{-4/9}$	1.782	1.712
E	Diemer & Olson (2002)	3	$(v^*)^{1/4} (1 - v^*)^{3/2}$	1.269	1.253
F	Diemer & Olson (2002)	4	$(v^*)^{1/2} (1 - v^*)^{7/2}$	1.190	1.185

Table 1: Daughter distributions used in Monte Carlo simulations and corresponding daughter-distribution constants C_f defined by equation (3.17) versus C_f^* defined by Gaylo *et al.* (2021, eq. (4.3)). Note, a constant to ensure $\int f_V^*(v^*) dv^* = 1$ is omitted for brevity.

310 from \bar{m} through a daughter-distribution constant C_f , defined as the ratio between C_τ and a
 311 C_τ found using the same \bar{m} but identical fragmentation, $f_V^*(v^*) = \delta(v^* - 1/\bar{m})$, where δ is
 312 the Dirac delta function. This gives

$$313 \quad C_\tau = \frac{C_f/C_{\Omega,\infty}}{1 - \bar{m}^{-2/9}}; \quad C_f = \frac{1 - \bar{m}^{-2/9}}{1 - \bar{m} \int_0^1 v^{*11/9} f_V^*(v^*) dv^*}. \quad (3.17a, b)$$

314 In table 1 we compare this C_f for general fragmentation cascades to the similar constant
 315 (hereafter denoted as C_f^*) derived by Gaylo *et al.* (2021) for the special case of power-
 316 law entrainment. The values are nearly equivalent, and, noting that $(9/2)(\ln \bar{m})^{-1} \approx (1 -$
 317 $\bar{m}^{-2/9})^{-1}$, (3.17) predicts similar τ_c as Gaylo *et al.* (2021) for their special case.

318 3.4. Measurement-interval independence of volume-propagation speed

319 A consequence of \bar{s} being constant for $a_p(t) > a_H$ is that the time-averaged value and the
 320 instantaneous speed are equal, $\mathbb{E}\{\langle s(t) \rangle_T\} = \bar{s}$, so long as $a_p(t+T) > a_H$. Thus, to obtain
 321 \bar{s} we must choose a T such that $\Pr\{a(t+T) > a_H\} \approx 1$. For measurements of an initial
 322 parent-bubble radius $a = a_p(t)$, we define an upper bound T_U as the interval we expect
 323 $a_p(t+T_U) \sim a_H$ and require $T \ll T_U$. Through the same arguments used to derive τ_c , this
 324 upper bound is

$$325 \quad T \ll \varepsilon^{-1/3} a^{2/3} C_\tau \left[1 - (We/We_H)^{-2/5} \right], \quad (3.18)$$

326 or simply $T \ll \tau_c$ for $a = a_{max}$. From Monte Carlo simulations of prescribed fragmentation
 327 statistics measuring initial bubbles $a = a_{max}$, figure 3 confirms that $\mathbb{E}\{\langle s \rangle_T\}$ gives an
 328 exact, T -independent measurement of \bar{s} for $T \ll \tau_c$. T_U provides an upper bound on T for
 329 experiments or simulations, although we point out that it is an *a posteriori* measure because
 330 C_τ is derived from \bar{s} .

331 Finally, T -independence means $d\mathbb{E}\{\langle s(t) \rangle_T\} / dT = 0$. As can be seen by taking the
 332 derivative of (3.13) with T^* , this bounds how scale-invariant fragmentation statistics $\bar{m}(T^*)$
 333 and $f_V^*(v^*; T^*)$ can depend on T^* and provides insight into the relationship between $\bar{m}(T^*)$
 334 and $f_V^*(v^*; T^*)$ measured at large T^* versus the theoretical $T^* \rightarrow 0$ limiting case used in PBE.
 335 This is useful because a finite relaxation time τ_r implies a lower bound ($T > \tau_r$) for measuring
 336 fragmentation statistics that are compatible with the PBE no-hysteresis assumption.

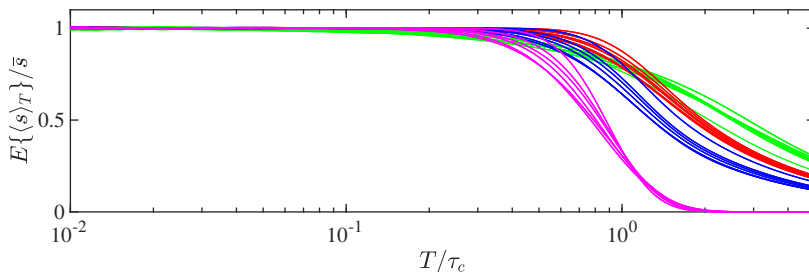


Figure 3: Measurements of $\mathbb{E}\{\langle s \rangle_T\}$ from Monte Carlo simulations of daughter distributions A-F (see table 1) at a range of T/τ_c , normalised by \bar{s} calculated using (3.14). Colours based on We^* : green, 2; red, 50; blue, 100; magenta, 200, where (3.1) is used to model the Hinze scale. The 95% C.I. on $\mathbb{E}\{\langle s \rangle_T\}$ for $T/\tau_c < 1$ is $< 3\%$.

We_T	We	Δ/η	We_Δ	Δ/a_H	N_{sims}	N_{frag}	C_Ω	C_τ
400	101 – 142	1.1	0.66	0.71	7	213	1.64 ± 0.42	8.9 ± 1.9
200	50 – 71	2.2	0.66	0.93	7	106	0.60 ± 0.13	16.1 ± 2.9
		1.5	0.44	0.62	7	189	1.21 ± 0.34	10.2 ± 2.5
		1.1	0.33	0.47	7	208	1.64 ± 0.44	9.8 ± 2.8
		0.7	0.22	0.31	5	187	1.77 ± 0.26	10.3 ± 2.1
100	25 – 36	1.1	0.16	0.31	7	218	1.50 ± 0.27	10.0 ± 2.3
50	13 – 18	1.1	0.08	0.20	7	174	0.93 ± 0.13	15.2 ± 2.9
25	6.3 – 8.9	1.1	0.04	0.13	7	113	0.44 ± 0.12	27.1 ± 5.5

Table 2: Summary of HIT simulations performed and values measured using $T/t_\ell = 0.4$, including 95% C.I.. N_{sims} is the number of simulations (each with different initial bubble populations) and N_{frag} is the total number of fragmentation events. a_H is calculated using $We_H \approx 7$ from §4.4.

337 4. Quantification of fundamental timescales using DNS

338 We perform direct numerical simulation (DNS) of populations of bubbles fragmenting in
 339 HIT to measure the relaxation time τ_r and bubble lifetime τ_ℓ , validate the T -independence
 340 of measurements of \bar{s} , and provide a value of C_τ along with the minimum We above which
 341 this value is valid. A summary of the DNS performed is provided in table 2.

342

4.1. Methodology

343 For DNS, we solve the three-dimensional, incompressible, immiscible, two-phase, Navier-
 344 Stokes equations using a second-order finite-volume scheme on a uniform Cartesian grid.
 345 Phases are captured by the conservative volume-of-fluid method (cVOF) (Weymouth & Yue
 346 2010), and surface tension is calculated using a height-function based continuous-surface-
 347 force method (Popinet 2009). More detail on the DNS solver is provided by Campbell (2014)
 348 and Yu *et al.* (2019). During the simulation, normals-based Informed Component Labeling
 349 (ICL) (Hendrickson *et al.* 2020) identifies bubbles, the air volumes of which are then tracked
 350 using Eulerian Label Advection (ELA) (Gaylo *et al.* 2022).

351 To develop the initial turbulent velocity field for the simulation, we use a linear forcing

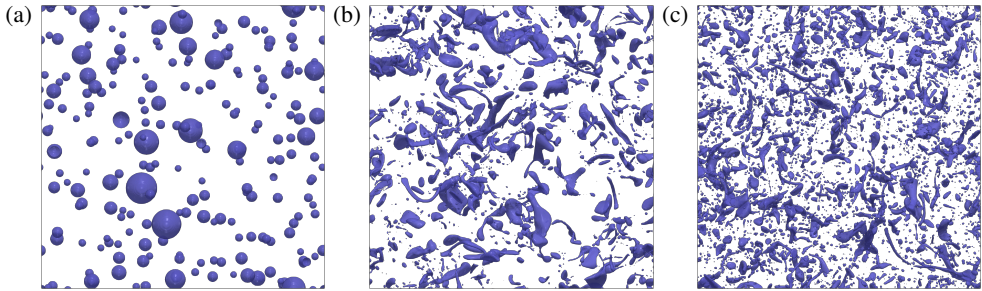


Figure 4: Volume-of-fluid $f = 0.5$ iso-surface for one of the $We_T = 100$ simulations at: (a) $t/t_\ell = 0$; (b) $t/t_\ell = 1$; (c) $t/t_\ell = 3$.

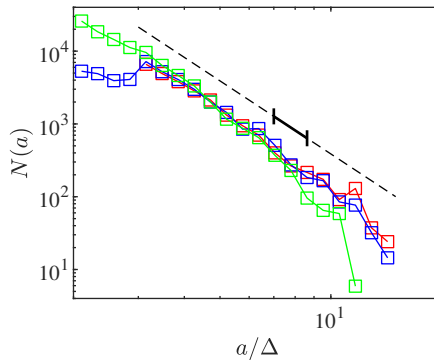


Figure 5: Average bubble-size distribution $N(a)$ for $We_T = 100$ simulations at times: red, $t/t_\ell = 0$; blue, $t/t_\ell = 1$; green, $t/t_\ell = 3$. $N(a) \propto a^{-10/3}$ is provided for reference over the range of initialised spherical bubbles (---) and the range of measured parent bubbles, $a_0 < a < 1.2a_0$ (—).

352 method (Lundgren 2003; Rosales & Meneveau 2005) on a triply periodic cubic domain, length
 353 $L = 5.28$, to develop single-phase HIT with a (non-dimensionalized) characteristic turbulent
 354 dissipation rate $\varepsilon = 1$, velocity fluctuation $u_{\text{rms}} = 1$, and Reynolds number $Re_T = u_{\text{rms}}^4 / \varepsilon \nu_w =$
 355 200 . Using the single-phase HIT as the initial velocity field, we perform simulations with
 356 an ensemble of different initial air-water bubble populations (density ratio $\rho_w / \rho_a = 1000$,
 357 viscosity ratio $\mu_w / \mu_a = 100$, void fraction 1%) at a range of turbulent Weber numbers,
 358 $We_T = \rho_w u_{\text{rms}}^5 / \varepsilon \sigma$. Although the abrupt introduction of bubbles to single-phase HIT is
 359 non-physical, numerical simulations rapidly adjust (Yu *et al.* 2019; Rivière *et al.* 2021).
 360 Populations are created by randomly distributing (without overlap) spherical bubbles with
 361 radii between $3L/256$ and $15L/256$ following $N(a) \propto a^{-10/3}$. By repeating the random
 362 generation and distribution of bubble populations in the initial HIT velocity field, unique but
 363 statistically similar initial bubble populations are generated to provide statistical variation
 364 between our ensemble simulations.

365 During the evolution, linear forcing is applied to regions of water to maintain $\varepsilon \approx 1$
 366 (Rivière *et al.* 2021). Figure 4 shows the evolution of a sample simulation and figure 5 shows
 367 the evolution of the ensemble bubble-size distribution both for $We_T = 100$. We note that,
 368 with our focus on bubbles $a > a_H$, the transition to a distinct power-law regime for $N(a < a_H)$
 369 is not captured (Deane & Stokes 2002). Over a measurement interval t^n to $t^{n+1} = t^n + T$, ELA
 370 provides the unique, volume-conservative volume-tracking matrix, where each element a_{ij}
 371 describes the volume that moved from a parent bubble j that is identified at t^n to a bubble i

372 identified at t^{n+1} (Gaylo *et al.* 2022). From volume-tracking matrices, fragmentation statistics
 373 $\mathbb{E}\{\langle s \rangle_T\}$ and $p_{\text{frag}}(a; T)$ can easily be computed.

374 We study fragmentation statistics for parent bubbles of radii $a_0 < a < 1.2a_0$, where
 375 $a_0 = 7L/256$ provides a balance between the number of observed fragmentation events
 376 per simulation and resolution of the daughter bubbles. While this simulation is inherently
 377 transient, figure 5 illustrates that for this range of bubbles a quasi-steady period exists.
 378 By initialising the bubbles to follow an equilibrium fragmentation cascade $N(a) \propto a^{-10/3}$
 379 (Garrett *et al.* 2000), the fragmentation of bubbles $a > a_0$ maintains the population of bubbles
 380 $a \sim a_0$ for $t/t_\ell < 3$, where $t_\ell = (0.42)^{-1} \varepsilon^{-1/3} a_0^{2/3}$ is an *a priori* estimate of τ_ℓ (Martínez-
 381 Bazán *et al.* 1999a). To exclude the fragmentation of the initial set of spherical bubbles
 382 (see figure 4), we study fragmentation over $1 < t/t_\ell$. Thus, by measuring fragmentation
 383 statistics over $1 < t/t_\ell < 3$, we measure a quasi-steady population of parent bubbles that are
 384 realistically formed by a fragmentation cascade.

385 4.2. Grid independence

386 The choice of cell size, Δ , is driven by resolving the relevant scales of turbulence and surface
 387 tension. For turbulence, we compare the grid to the Kolmogorov micro scale, $\eta \sim \varepsilon^{-1/4} \nu_w^{3/4}$,
 388 where $\Delta/\eta \lesssim 1$ ensures turbulence is resolved. For surface tension, we consider the cell Weber
 389 number $We_\Delta = \rho_w u_{\text{rms}}^2 \Delta / 4\pi\sigma$, which estimates the ratio between the grid and the minimum
 390 characteristic radius of curvature of an interface deformed by inertial turbulence. $We_\Delta < 1$
 391 ensures surface tension forces are resolved by the grid (Popinet 2018). We also consider
 392 Δ/a_H , comparing the grid to the Hinze scale: with ε and u_{rms} fixed $We_\Delta^{3/5} \propto \Delta/a_H$. Based
 393 on these metrics we find $L/\Delta = 256$ resolves turbulence and surface tension for our entire
 394 range of We_T (see table 2).

395 With no clear lower limit to the ratio between the daughter-bubble and parent-bubble
 396 volume (v^*), grid resolution limitations require us to filter out daughter bubbles of radius
 397 $a < 2\Delta$. Figure 7 shows that the bubble-size distribution of filtered bubbles, $N(a > 2\Delta)$, is
 398 grid-independent. For $L/\Delta = 256$ and parent bubbles $a_0 = 7L/256$, $a < 2\Delta$ corresponds to
 399 $v^* < 0.02$. While this filter prevents us from measuring the full range of possible daughter
 400 bubbles, especially sub-Hinze daughters, we expect this to have little effect on the statistics
 401 of interest for two reasons. First, sub-Hinze bubble production by fragmentation happens
 402 concurrently with the production of large daughter bubbles (Rivière *et al.* 2022), so excluding
 403 small daughters should not affect the measured rate of fragmentation used to obtain τ_r and
 404 τ_ℓ . Second, for τ_c , the integral of the daughter-size distribution in (3.17) weights local
 405 daughter production ($v^* \sim 1/\bar{m}$) over non-local daughter production ($v^* \ll 1$), making the
 406 contribution of the excluded small daughters small. This is related conceptually to locality,
 407 which suggests $v^* \ll 1$ can be neglected when modelling the cascade (Chan *et al.* 2021b,c).

408 To confirm that we resolve turbulence and surface tension, that the filter has a negligible
 409 effect, and (more broadly) that the statistics we measure are independent of the grid, we
 410 perform a convergence study for $We_T = 200$ using three additional grids, $L/\Delta = 128, 192,$
 411 and 384. The results of this convergence study (see figure 6) show that our measurements
 412 of fragmentation statistics $\mathbb{E}\{\langle s \rangle_T\}$ and $p_{\text{frag}}(a; T)$ (from which the timescales will be
 413 calculated) are grid independent for $L/\Delta \geq 256$.

414 4.3. Estimating relaxation time, τ_r

415 For each simulation, we use 6 instances of ELA with different measurement intervals T .
 416 Using (2.4) and (2.7), we calculate $C_Q(We; T)$ from each $p_{\text{frag}}(a; T)$. Figure 8a shows how
 417 T affects the measured value of C_Q , where we use $T/t_\ell = 0.4$ as a reference value for each
 418 We . If the no-hysteresis assumption were valid for all T , C_Q would be a constant for each We .

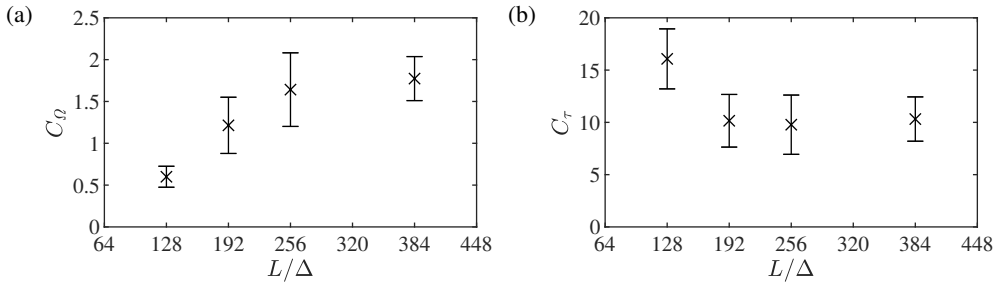


Figure 6: Grid-convergence study for (a) fragmentation rate constant C_Q and (b) convergence constant C_T based on simulations of $We_T = 200$ (parent bubbles $We = 50 - 71$) with different grids, measured using $T/t_\ell = 0.4$. Error bars indicate 95% C.I..

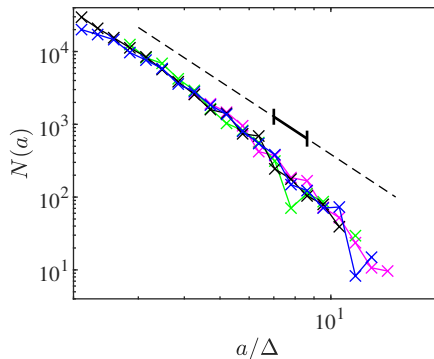


Figure 7: Average bubble-size distribution $N(a > 2\Delta)$ for $We_T = 200$ at time $t/t_\ell = 3$ from simulations with grids: magenta, $L/\Delta = 128$; green, $L/\Delta = 192$; black, $L/\Delta = 256$; blue, $L/\Delta = 384$; Horizontal axis is normalised by $\Delta = L/256$ and $N(a) \propto a^{-10/3}$ is provided for reference over the range of initialised spherical bubbles (---) and the range of measured parent bubbles, $a_0 < a < 1.2a_0$ (—).

419 Figure 8a however shows a strong dependence on small T . We observe that this dependence
 420 is approximately exponential, which provides an empirical definition of the relaxation time
 421 τ_r as well as the hysteresis strength A :

$$422 \quad C_Q(We; T)/C_Q(We; T \sim \infty) = 1 + A \exp[-T/\tau_r] . \quad (4.1)$$

423 We observe that τ_r scales like τ_ℓ rather than, say, bubble natural period, $We^{-1/2}\varepsilon^{-1/3}a^{2/3}$.
 424 Thus, we define the scaling constant C_r and write $\tau_r = C_r\varepsilon^{-1/3}a^{2/3}$. This scaling suggests
 425 that, for $We > We_H$, the physical mechanisms for the decay of hysteresis are not related
 426 to surface tension. Future, more detailed, studies of the dynamics of individual bubbles
 427 are necessary to understand hysteresis and identify the mechanisms for its decay. For our
 428 statistical study, our concern is to determine when hysteresis can be neglected. Least-squares
 429 regression of the combined data for all We gives $C_r \approx 0.11$. Hereafter, we measure all results
 430 with $T/t_\ell = 0.4$ (corresponding to $T/\tau_r \approx 8$), which guarantees that effect of hysteresis on
 431 our estimation of τ_ℓ and τ_c is negligible.

432 4.4. Estimating bubble lifetime, τ_ℓ

433 We now seek the expected bubble lifetime, τ_ℓ . Figure 9a shows our measurements of $C_Q(We)$
 434 and their fit to (2.5). We find the Hinze-scale $We_H = 6.9$, similar to $We_H = 4.7$ measured by

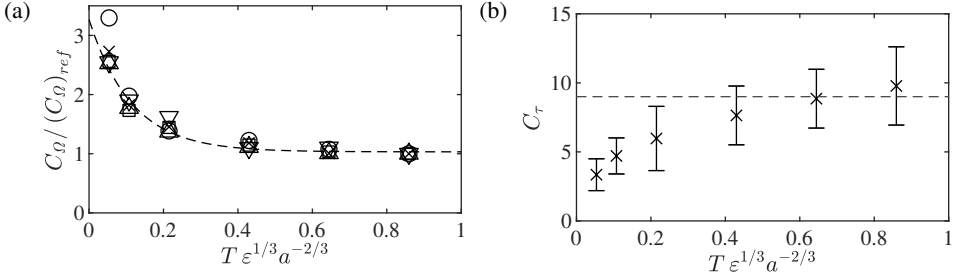


Figure 8: Measured (a) fragmentation-rate constant C_Q normalised by $(C_Q)_{ref}$, the value measured using $T/t_\ell = 0.4$ and (b) the convergence constant C_τ for We of (O) 101 – 142; (x) 50 – 71; (□) 25 – 36; (△) 13 – 18; (▽) 6.3 – 8.9. In (a), variance-weighted least-squares fit of all data to (4.1) (---) gives $C_r = 0.11$ and $A = 2.2$ ($R^2 = 0.954$). In (b), error bars indicate 95% C.I. and the estimated large- We value of $C_\tau = 9$ (---) is included for reference.

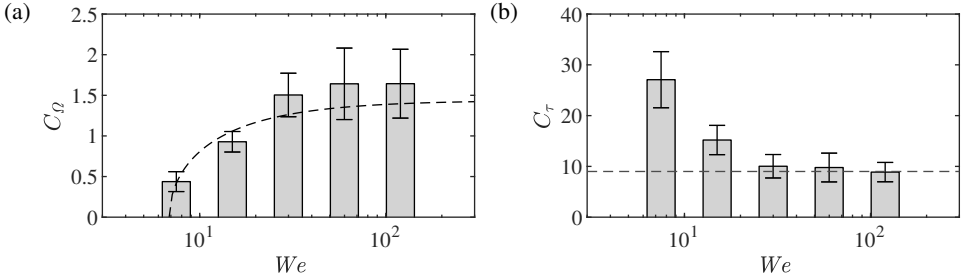


Figure 9: (a) Fragmentation rate constant C_Q and (b) convergence constant C_τ as functions of We , measured using $T/t_\ell = 0.4$. Error bars indicate 95% C.I.. In (a), variance-weighted least-squares fit to (2.5) (---) gives $We_H = 6.9$ and $C_{Q,\infty} = 1.4$ ($R^2 = 0.890$). In (b), the estimated large- We value of $C_\tau = 9$ (---) is included for reference.

435 Martínez-Bazán *et al.* (1999a) and $We_H = 2.7 - 7.8$ by Risso & Fabre (1998). However, we
 436 obtain $C_{Q,\infty} = 1.4$, greater than $C_{Q,\infty} = 0.42$ measured by Martínez-Bazán *et al.* (1999a)
 437 and $C_{Q,\infty} = 0.95$ from HIT simulations by Rivière *et al.* (2021). An important distinction
 438 between our fragmentation rate measurements and previous experimental and numerical
 439 measurements is that we measure bubbles that have been formed as the daughters of previous
 440 fragmentation, so the bubbles are already distorted by fragmentation. The effect of this
 441 distinction can be demonstrated by measuring the fragmentation statistics over an earlier
 442 time in our simulation, $0 < t/t_\ell < 1$, when (as opposed to the later time $1 < t/t_\ell < 3$)
 443 many parent bubbles which started spherical have not yet fragmented. When we measure this
 444 earlier time range (denoted by $(\cdot)_{t < t_\ell}$), we obtain a similar $(We_H)_{t < t_\ell} = 7.0$ but an appreciably
 445 smaller $(C_{Q,\infty})_{t < t_\ell} = 0.88$ ($R^2 = 0.974$). As our interest is bubbles *within* fragmentation
 446 cascades, our value of $C_{Q,\infty} \approx 1.4$ is more relevant for bubbles formed by fragmentation.
 447 Note that $1/C_{Q,\infty}$ is an order of magnitude larger than C_r (i.e., $\tau_\ell \gg \tau_r$), which confirms that
 448 the PBE no-hysteresis assumption is reasonable when modelling fragmentation cascades.

449

4.5. Estimating convergence time, τ_c

450 We now seek the convergence time, τ_c . As shown in §3, the time-averaged speed $\mathbb{E}\{\langle s \rangle_T\}$,
 451 available from ELA, gives a T -independent measurement of C_τ so long as (3.18) is satisfied.
 452 Figure 9b shows the value of C_τ we obtain over a range of We . We find that the model

453 developed in §3, which as a result of large- We assumptions predicts a constant C_τ , is accurate
 454 for $We \gg We_H$, or more specifically $We > 30$, where we measure $C_\tau \approx 9$. To validate that
 455 our measurement is T -independent, we also measure C_τ using a range of T for $We = 50 - 71$
 456 (figure 8b). As expected, for $T \lesssim \tau_r$ we see a dependence on T due to hysteresis, but for
 457 $T \gg \tau_r$ C_τ is independent of T . Using $C_\tau = 9$, (3.18) gives $T/T_U < 0.2$ for $We > 30$, so we
 458 do not expect any effect of the Hinze scale driven upper bound on T -independence described
 459 in §3.4.

460 5. Discussion

461 We now examine how the relaxation time τ_r , bubble lifetime τ_ℓ , and convergence time τ_c
 462 inform the study of fragmentation. For τ_r , our results suggest that the physical mechanism
 463 for the decay of hysteresis with bubble age is independent of surface tension for $We >$
 464 We_H and that τ_r scales like τ_ℓ . The respective scaling constants we estimate from DNS
 465 of HIT differ by an order of magnitude ($C_r \ll 1/C_{\Omega,\infty}$), suggesting that $\tau_r \ll \tau_\ell$ is
 466 always true for $We > We_H$. Although the physical mechanism for the decay of hysteresis is
 467 unclear, this shows that hysteresis can be assumed negligible when modelling fragmentation,
 468 validating an essential assumption of PBE. More practically, knowledge of τ_r also informs
 469 the choice of measurement interval in experiments and simulations. $T \gg \tau_r$ makes the effect
 470 of hysteresis on measurements negligible, ensuring that the measured fragmentation statistics
 471 are compatible with PBE.

472 The insight that the convergence time τ_c provides into the evolution of the bubble-size
 473 distribution in fragmentation-dominated bubbly flows has been discussed by Qi *et al.* (2020)
 474 and Deike *et al.* (2016), and we have now quantified τ_c directly. For large We where the effect
 475 of surface tension on fragmentation rates is negligible, we find

$$476 \quad \tau_c = C_\tau \varepsilon^{-1/3} a_{max}^{2/3} \left[1 - (We_{max}/We_H)^{-2/5} \right], \quad (5.1)$$

477 where We_{max} is the Weber number of the largest bubble in the cascade (radius a_{max}) and we
 478 estimate $C_\tau \approx 9$ and $We_H \approx 6.9$ from DNS. In addition, as we can now express τ_c in terms
 479 of realistic fragmentation statistics for $We > 30$, τ_c also informs large- We fragmentation
 480 models. Inspired by (2.3), we rearrange (3.17) to provide a new bound on a moment of the
 481 daughter-size distribution f_V^* :

$$482 \quad \bar{m} \int_0^1 v^{*11/9} f_V^*(v^*) dv^* = 1 - (C_\tau C_{\Omega,\infty})^{-1}, \quad (5.2)$$

483 where our estimations of $C_\tau \approx 9$ and $C_{\Omega,\infty} = 1.4$ from DNS give 0.92 for the right-hand side
 484 of (5.2). For a physical interpretation, (2.3) bounds the relationship between daughter-size
 485 distributions and \bar{m} to guarantee volume conservation, while (for $We > 30$) (5.2) bounds the
 486 relationship to match the empirical value of τ_c .

487 Many existing fragmentation models assume binary breakup ($\bar{m} = 2$). To evaluate how well
 488 these meet (5.2), we focus on the proposed daughter-size distributions through C_f , which
 489 includes the integral in (5.2). With $\bar{m} = 2$, $C_\tau \approx 9$, and $C_{\Omega,\infty} = 1.4$, we obtain $C_f \approx 1.8$.
 490 Because C_f indicates how much longer τ_c is compared to the case of identical fragmentation,
 491 this shows that τ_c is 1.8 times longer for fragmentation in HIT than what would be predicted
 492 if one assumes identical binary-fragmentation. Comparing to more realistic binary daughter-
 493 distributions (B-D in table 1), we see good agreement with the distribution proposed by
 494 Martínez-Bazán *et al.* (2010). We also compare to the binary daughter-distribution model
 495 by Qi *et al.* (2020, eq. (7)), which uses an experimentally-constrained fitting parameter
 496 $\omega = 0.3$ designed to tune the value of τ_c . For their daughter-distribution model, (3.17) gives

497 $C_f = 1.741$, in good agreement with our value of $C_f \approx 1.8$. Although we assume $\bar{m} = 2$ here
 498 for illustration, this analysis is applicable to any \bar{m} . Rather than attempting to compare the
 499 details of disparate fragmentation models, relating τ_c to the fragmentation statistics specified
 500 by these models allows us to directly compare the physical predictions each model makes
 501 regarding the evolution of the bubble-size distribution through a simple scalar quantity.

502 6. Conclusion

503 For air-water bubbly flows under HIT at moderate to large Weber numbers, we describe
 504 three fundamental timescales characterising the statistics of the evolution of the bubble-size
 505 distribution by fragmentation and the resulting fragmentation cascade. The prevalence of the
 506 observation of $-10/3$ power-law in bubble-size distributions in bubbly flow for moderate
 507 and large We demonstrates the importance of fragmentation cascades to the bubble-size
 508 distribution, and these timescales directly support statistical modelling of fragmentation.
 509 Although our focus here is on statistical descriptions of fragmentation, the results here also
 510 help inform mechanistic study of fragmentation.

511 One fundamental timescale is the relaxation time τ_r which characterises the time after
 512 fragmentation over which hysteresis cannot be neglected. From DNS measurements, we
 513 provide an empirical definition of τ_r based on when measured fragmentation rates become
 514 independent of the measurement interval T . We find that $\tau_r = C_r \varepsilon^{-1/3} a^{2/3}$, where $C_r \approx 0.11$
 515 independent of moderate/large We . This We -independence suggests the physical mechanism
 516 causing τ_r at these We is unrelated to surface tension. Although understanding hysteresis and
 517 its decay is an area of future work, by providing τ_r we identify the timescales over which
 518 hysteresis can be neglected.

519 A second fundamental timescale is the expected lifetime τ_ℓ of a bubble from formation
 520 by fragmentation to further fragmentation. For $\tau_\ell \gg \tau_r$, $\tau_\ell = [C_\Omega(We)]^{-1} \varepsilon^{-1/3} a^{2/3}$ is the
 521 inverse of the fragmentation rate. Fitting our DNS results for bubbles within the fragmentation
 522 cascade to the square-root model of We -dependence by Martínez-Bazán *et al.* (1999a)
 523 (eq. (2.5)), we find the Hinze-scale $We_H \approx 6.9$, in agreement with previous experiments, but
 524 measure a smaller τ_ℓ corresponding to a higher scaling constant (at large We) $C_{\Omega,\infty} \approx 1.4$
 525 (compared to $C_{\Omega,\infty} \approx 0.42$ reported by Martínez-Bazán *et al.* (1999a)). We show that this
 526 higher value of $C_{\Omega,\infty}$ is related to formation of the bubbles by a fragmentation cascade. For
 527 modelling fragmentation cascades, this higher $C_{\Omega,\infty}$ is likely more relevant. In either case,
 528 we find $\tau_r \ll \tau_\ell$ for all We , validating the use of the no-hysteresis assumption in modelling
 529 fragmentation.

530 Finally, we consider the fundamental timescale $\tau_c = C_\tau [1 - (We_{max}/We_H)^{-2/5}] \varepsilon^{-1/3} a_{max}^{2/3}$,
 531 which measures the time for a Lagrangian air particle to go from the largest bubble to
 532 the Hinze scale. This also characterises the time for fragmentation cascades to reach
 533 equilibrium. For large We , we derive τ_c based on the (constant) expected speed \bar{s} at which
 534 a Lagrangian air particle moves through the cascade. We show that, $C_\tau = 1/\bar{s}$ and can
 535 thus be measured independent of T . This result is valid for $\tau_r \ll T \ll \tau_c$, which provides
 536 a bound on the choice of T in experiments and simulations. The T -independence of C_τ
 537 is confirmed by DNS measurements, which give $C_\tau \approx 9$ for $We > 30$, which agrees well
 538 with the values obtained from the fragmentation model of Martínez-Bazán *et al.* (2010) and
 539 an experimentally-constrained fragmentation model of Qi *et al.* (2020). The relationship
 540 between C_τ and fragmentation statistics in PBE provides new constraints on these statistics,
 541 at large We , limiting the possible forms of fragmentation models. Further, by quantifying C_τ ,
 542 we obtain the convergence time of fragmentation cascades τ_c , beyond which a quasi-steady
 543 model of fragmentation would be appropriate.

544 **Funding.** This work was funded by the U.S. Office of Naval Research grant N00014-20-1-2059 under the
 545 guidance of Dr. W.-M. Lin. The computational resources were funded through the Department of Defense
 546 High Performance Computing Modernization Program.

547 **Declaration of Interests.** The authors report no conflict of interest.

REFERENCES

- 548 CAMPBELL, B. 2014 A Mechanistic Investigation of Nonlinear Interfacial Instabilities Leading to Slug
 549 Formation in Multiphase Flows. PhD thesis, MIT.
- 550 CASTRO, A. M. & CARRICA, P. M. 2013 Bubble size distribution prediction for large-scale ship flows: Model
 551 evaluation and numerical issues. *Int. J. Multiphase Flow* **57**, 131–150.
- 552 CHAN, W. H. R., DODD, M. S., JOHNSON, P. L. & MOIN, P. 2021a Identifying and tracking bubbles and drops
 553 in simulations: A toolbox for obtaining sizes, lineages, and breakup and coalescence statistics. *J.*
 554 *Comput. Phys.* **432**, 110156.
- 555 CHAN, W. H. R., JOHNSON, P. L. & MOIN, P. 2021b The turbulent bubble break-up cascade. Part 1. Theoretical
 556 developments. *J. Fluid Mech.* **912**, A42.
- 557 CHAN, W. H. R., JOHNSON, P. L., MOIN, P. & URZAY, J. 2021c The turbulent bubble break-up cascade. Part
 558 2. Numerical simulations of breaking waves. *J. Fluid Mech.* **912**, A43.
- 559 DEANE, G. B. & STOKES, M. D. 2002 Scale dependence of bubble creation mechanisms in breaking waves.
 560 *Nature* **418**, 839–844.
- 561 DEIKE, L. 2022 Mass Transfer at the Ocean–Atmosphere Interface: The Role of Wave Breaking, Droplets,
 562 and Bubbles. *Annu. Rev. Fluid Mech.* **54** (1), 191–224.
- 563 DEIKE, L., MELVILLE, W. K. & POPINET, S. 2016 Air entrainment and bubble statistics in breaking waves. *J.*
 564 *Fluid Mech.* **801**, 91–129.
- 565 DIEMER, R. B. & OLSON, J. H. 2002 A moment methodology for coagulation and breakage problems: Part
 566 3—generalized daughter distribution functions. *Chem. Eng. Sci.* **57**, 4187–4198.
- 567 GARRETT, C., LI, M. & FARMER, D. 2000 The connection between bubble size spectra and energy dissipation
 568 rates in the upper ocean. *J. Phys. Oceanogr.* **30** (9), 2163–2171.
- 569 GAYLO, D. B., HENDRICKSON, K. & YUE, D. K. 2021 Effects of power-law entrainment on bubble
 570 fragmentation cascades. *J. Fluid Mech.* **917**, R1.
- 571 GAYLO, D. B., HENDRICKSON, K. & YUE, D. K. 2022 An Eulerian label advection method for conservative
 572 volume-based tracking of bubbles/droplets. *J. Comput. Phys.* **470**, 111560.
- 573 HENDRICKSON, K., WEYMOUTH, G. D. & YUE, D. K. 2020 Informed component label algorithm for robust
 574 identification of connected components with volume-of-fluid method. *Comput. Fluids* **197**, 104373.
- 575 HINZE, J. O. 1955 Fundamentals of the hydrodynamic mechanism of splitting in dispersion processes. *AIChE*
 576 *J.* **1**, 289–295.
- 577 LIAO, Y. & LUCAS, D. 2009 A literature review of theoretical models for drop and bubble breakup in turbulent
 578 dispersions. *Chem. Eng. Sci.* **64**, 3389–3406.
- 579 LUNDGREN, T. S. 2003 Linearly forced isotropic turbulence. *Tech. Rep.*. Center for Turbulence Research,
 580 Stanford University.
- 581 MARTÍNEZ-BAZÁN, C., MONTAÑÉS, J. L. & LASHERAS, J. C. 1999a On the breakup of an air bubble injected
 582 into a fully developed turbulent flow. part 1. breakup frequency. *J. Fluid Mech.* **401**, 157–182.
- 583 MARTÍNEZ-BAZÁN, C., MONTAÑÉS, J. L. & LASHERAS, J. C. 1999b On the breakup of an air bubble injected
 584 into a fully developed turbulent flow. part 2. size pdf of the resulting daughter bubbles. *J. Fluid Mech.*
 585 **401**, 183–207.
- 586 MARTÍNEZ-BAZÁN, C., RODRÍGUEZ-RODRÍGUEZ, J., DEANE, G. B., MONTAÑÉS, J. L. & LASHERAS, J. C. 2010
 587 Considerations on bubble fragmentation models. *J. Fluid Mech.* **661**, 159–177.
- 588 POPINET, S. 2009 An accurate adaptive solver for surface-tension-driven interfacial flows. *J. Comput. Phys.*
 589 **228** (16), 5838–5866.
- 590 POPINET, S. 2018 Numerical Models of Surface Tension. *Annu. Rev. Fluid Mech.* **50** (1), 49–75.
- 591 QI, Y., MOHAMMAD MASUK, A. U. & NI, R. 2020 Towards a model of bubble breakup in turbulence through
 592 experimental constraints. *Int. J. Multiphase Flow* **132**, 103397.
- 593 QI, Y., TAN, S., CORBITT, N., URBANIK, C., SALIBINDLA, A. K. R. & NI, R. 2022 Fragmentation in turbulence
 594 by small eddies. *Nat. Commun.* **13** (1), 469.
- 595 RISSO, F. & FABRE, J. 1998 Oscillations and breakup of a bubble immersed in a turbulent field. *J. Fluid*
 596 *Mech.* **372**, 323–355.

- 597 RIVIÈRE, A., MOSTERT, W., PERRARD, S. & DEIKE, L. 2021 Sub-Hinze scale bubble production in turbulent
598 bubble break-up. *J. Fluid Mech.* **917**, A40.
- 599 RIVIÈRE, A., RUTH, D. J., MOSTERT, W., DEIKE, L. & PERRARD, S. 2022 Capillary driven fragmentation of
600 large gas bubbles in turbulence. *Phys. Rev. Fluids* **7** (8), 083602.
- 601 ROSALES, C. & MENEVEAU, C. 2005 Linear forcing in numerical simulations of isotropic turbulence: Physical
602 space implementations and convergence properties. *Phys. Fluids* **17**, 095106.
- 603 SKARTLIEN, R., SOLLUM, E. & SCHUMANN, H. 2013 Droplet size distributions in turbulent emulsions: Breakup
604 criteria and surfactant effects from direct numerical simulations. *J. Chem. Phys.* **139**, 174901.
- 605 SOLSVIK, J., MAAB, S. & JAKOBSEN, H. A. 2016 Definition of the Single Drop Breakup Event. *Ind. Eng.*
606 *Chem. Res* **55**, 2872–2882.
- 607 SPORLEDER, F., BORKA, Z., SOLSVIK, J. & JAKOBSEN, H. A. 2012 On the population balance equation.
608 *Reviews in Chemical Engineering* **28**, 149–169.
- 609 TSOURIS, C. & TAVLARIDES, L. L. 1994 Breakage and coalescence models for drops in turbulent dispersions.
610 *AIChE J.* **40**, 395–406.
- 611 VALENTAS, K. J., BILOUS, O. & AMUNDSON, N. R. 1966 Analysis of breakage in dispersed phase systems.
612 *Ind. Eng. Chem. Fundamen.* **5**, 271–279.
- 613 VEJRAŽKA, J., ZEDNÍKOVÁ, M. & STANOVSKÝ, P. 2018 Experiments on breakup of bubbles in a turbulent
614 flow. *AIChE Journal* **64**, 740–757.
- 615 WEYMOUTH, G. & YUE, D. K. 2010 Conservative Volume-of-Fluid method for free-surface simulations on
616 Cartesian-grids. *J. Comput. Phys.* **229** (8), 2853–2865.
- 617 YU, X., HENDRICKSON, K., CAMPBELL, B. K. & YUE, D. K. 2019 Numerical investigation of shear-flow
618 free-surface turbulence and air entrainment at large Froude and Weber numbers. *J. Fluid Mech.* **880**,
619 209–238.
- 620 YU, X., HENDRICKSON, K. & YUE, D. K. P. 2020 Scale separation and dependence of entrainment bubble-size
621 distribution in free-surface turbulence. *J. Fluid Mech.* **885**, R2.